Analysis of the Phase Current Measurement Boundary of Three Shunt Sensing PWM Inverters and an Expansion Method

Byung-Geuk Cho^a, Jung-Ik Ha^a and Seung-Ki Sul^a

^a Seoul National University School of Electrical Engineering & Computer Science, Seoul, Korea

bk8089@eepel.snu.ac.kr

Abstract — This paper deals with the derivation of the boundary conditions for phase current reconstruction and proposes a voltage injection method to expand the measurable areas in three-shunt sensing inverters. The boundary conditions are analyzed on the voltage vector plane for space vector pulse width modulation (SVPWM) and discontinuous pulse width modulation (DPWM). Once derived, the boundary areas are divided into sub-areas and different voltages are injected for each sub-area. In each sub-area, different minimum voltages are injected according to the position of the original voltage reference vector. The proposed method minimizes the current ripples produced by a voltage injection. Simulation and experimental results are presented to verify the boundary condition derivation and the effectiveness of the proposed voltage injection method.

Keywords — Current reconstruction, PWM inverters, Shunt resistor, Three-shunt sensing.

I. INTRODUCTION

Three-phase PWM inverters are widely used in industrial applications, especially in AC motor drive systems. In motor drives in which instantaneous torque control is required, phase currents flowing into the motor should be sensed. Thus far, much research on current sensing technologies such as shunts, current transformers, Rogowski coils, hall effect sensors, magneto impedance (MI) sensors, giant magneto resistive (GMR) sensors, pilot devices in power semiconductors and optical current sensors has been conducted [1]-[7]. Particularly, shunt measurements detect shoot-through or short circuit faults, showing excellent integration in the system. These are also known to be the most cost-effective measurement types. Accordingly, they are broadly used for home appliances or in general-purpose motor control systems despite the losses that arise from the shunt resistors and the fact that measurable phase currents are limited under certain conditions.

Fig. 1(a) and (b) show typical configurations of shunt output phase current sensing inverters. These two circuits are referred to as a three-shunt sensing inverter (TSSI) and a single-shunt sensing inverter (SSSI), respectively. In the SSSI, the output phase currents are reconstructed with the DC link current. The relationship between the DC link current and the phase current was initially

derived in [5]; since then, numerous methods of phase current reconstruction based on an adjustment of the switching pattern or on estimators have been reported [5]-[7]. However, the SSSI has an inherent disadvantage in that simultaneous current sampling for two phases is impossible, resulting in errors in the instantaneous threephase current information. In addition, because the DC shunt current must be measured when an effective vector is applied, the average current during the switching period cannot be sampled. On the other hand, the TSSI allows for an independent and simultaneous measurement of each phase current. However, this method is associated with losses of three-shunt resistors. Moreover, the efficiency is questionable in high-current applications. Nevertheless, TSSI is an attractive and broadly applicable inverter configuration due to its simple reconstruction process and potential integration of the sensor in the power semiconductor itself.

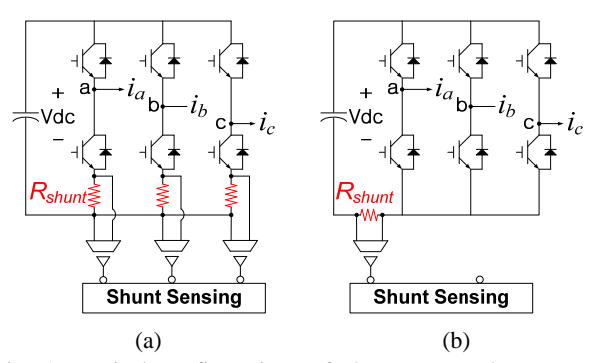


Fig. 1. Typical configurations of shunt output-phase current sensing inverters. : (a) Three-shunt sensing inverter (TSSI) and (b) single-sensing inverter (SSSI).

Essentially, shunt sensing inverters show limited levels of performance owing to their inherently defective phase current reconstruction capability depending on the operating condition. Various papers have attempted to identify and enhance the boundaries of the feasible phase current measurement range. However, most papers on the topic of shunt sensing inverters were unfortunately inclined towards SSSI; few works have examined TSSI.

This paper deals with TSSI and discusses its phase current measurement boundary. The boundary is obtained specifically with numerical formulas according to PWM schemes.

Based on the derivation, the phase current measurement range can be expanded. This paper proposed a voltage injection method based on that in [21] for SSSI. Although current ripples are generated due to the injected voltage, they can be minimized with the minimum magnitude voltage injection. Simulation and experimental results are provided to support the effectiveness of the works.

II. OPERATION BOUNDARY OF TSSI FOR PHASE CURRENT RECONSTRUCTION

A. Derivation of the Boundary Conditions

To reconstruct phase currents, the shunt currents need to be investigated. Fig. 2 depicts the circuit state of phase 'a' when the lower switch is on. As shown in the figure, the shunt current corresponds to the phase current regardless of the current's direction/polarity. In short, acquisition of the phase current information depends on the state of the lower switch; the measurable phase currents according to the switching states can be tabulated as shown in Table I for a three-phase voltage source inverter (VSI).

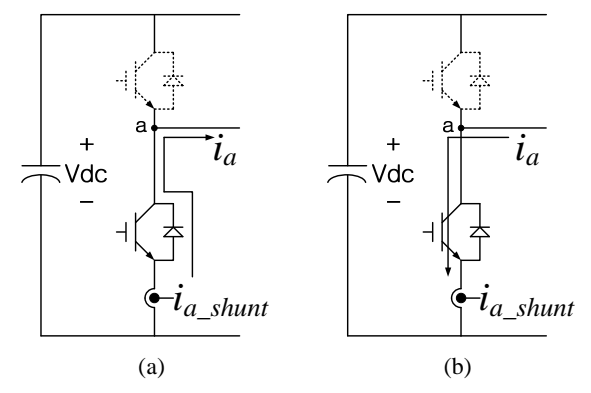


Fig. 2. Circuits state when the lower switch is on, (a) when positive current flows and (b) when negative current flows.

TABLE I

MEASURABLE PHASE CURRENTS DEPENDING ON THE SWITCHING
STATE

Switching state (Sa, Sb, Sc)	Shunt currents
(Sa, Sb, Sc)	$(i_{a \text{ shunt}}, i_{b \text{ shunt}}, i_{c \text{ shunt}})$
(1,0,0)	$\left(0,i_{_{b}},i_{_{c}} ight)$
(1,1,0)	$\left(0,0,i_{c} ight)$
(0, 1, 0)	$\left(i_a,0,i_c ight)$
(0, 1, 1)	$(i_a,0,0)$
(0,0,1)	$(i_a, i_b, 0)$
(1,0,1)	$(0,i_b,0)$
(0,0,0)	$\left(i_{a},i_{b},i_{c} ight)$
(1,1,1)	(0,0,0)

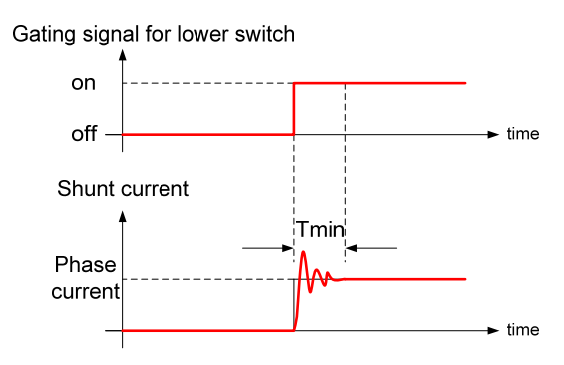
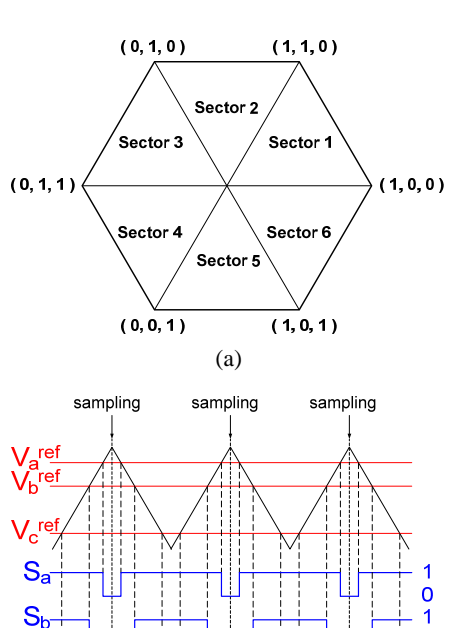


Fig. 3. Shunt current waveform.



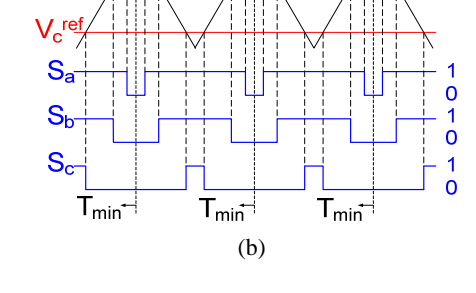


Fig. 4. Voltage vectors and corresponding switching patterns for SVPWM. : (a) Sector division of voltage plane and (b) switching patterns for sector 1.

In practice, when shunt currents are measured to reconstruct phase currents, the settling time of the shunt current must be considered. Due to the resonant effects caused by stray capacitances on the circuit and/or the reverse recovery of diodes, the shunt current is not identical to the phase current during 'Tmin', as shown in Fig. 3. Consequently, the shunt current must be measured at least 'Tmin' after the lower switch is turned on for accurate phase current reconstruction. This defines the boundary condition for TSSI.

Therefore, to reconstruct the phase current from a shunt current measurement after considering the given conditions, the switching patterns of an inverter should be identified. When SVPWM is applied for the PWM of a three-phase VSI, the switching patterns are determined according to the location of the voltage reference on the voltage plane, as defined in Fig. 4(a). Specifically, if the voltage vector is located in sector 1, the switching patterns of three phases are determined, as shown in Fig. 4(b). It can be deduced that the minimum duration 'Tmin' of the lower switches must be assured.

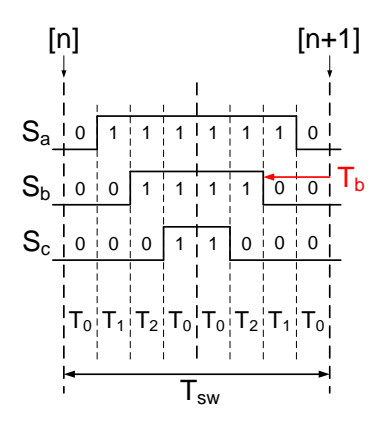


Fig. 5. Switching patterns in sector 1 for SVPWM.

$$T_b = T_0 + T_1 < T_{\min}$$
 (1)

$$2T_0 + T_1 + T_2 = \frac{T_{sw}}{2} \tag{2}$$

The result of equating (1) and (2), is as follows. :

$$T_2 > T_1 + \frac{T_{sw}}{2} - 2T_{min}$$
 (3)

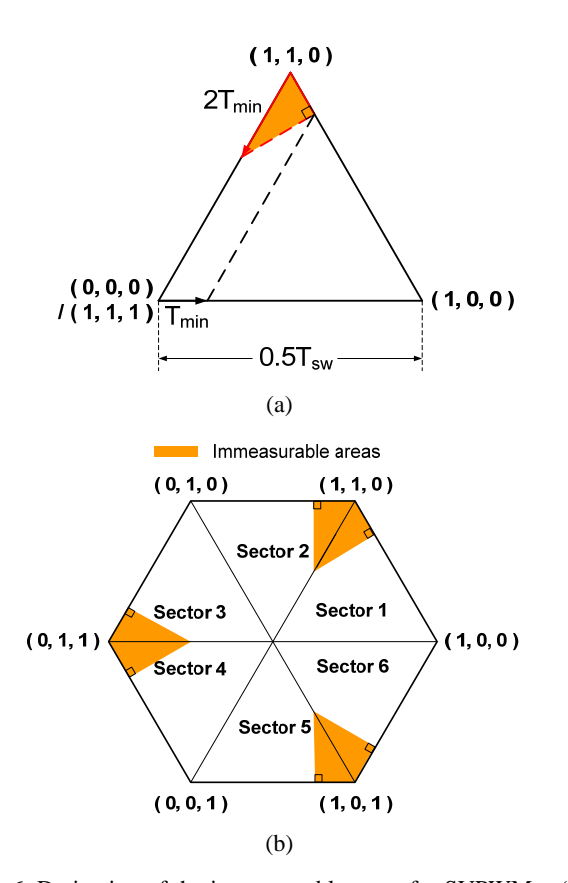


Fig. 6. Derivation of the immeasurable areas for SVPWM. : (a) Immeasurable area in sector 1, and (b) all immeasurable areas.

To derive the boundary conditions in sector 1 for TSSI considering the above restraint, the switching states are re-depicted in Fig. 5. Here, T_0 and T_1/T_2 denote the duration of the zero and effective vectors, respectively. In sector 1, it is not necessary to measure the shunt current of phase 'a', which has the shortest duration, because the currents of the two phases are enough to identify the currents of all three phases in the Y connection. Thus, T_b is required to be longer than 'Tmin' for the measurements of the shunt currents in phases 'b' and 'c'. Equations from (1) to (3) show the mathematical expressions of the boundary conditions in sector 1. The immeasurable areas are presented in yellow in Fig. 6.

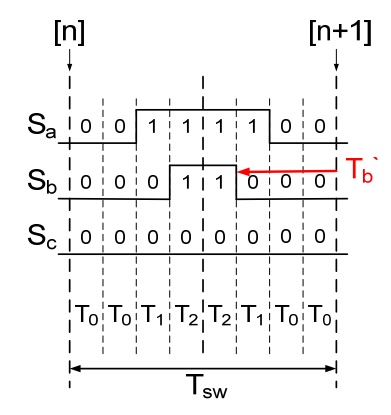


Fig. 7. Switching patterns in sector 1 for DPWM.

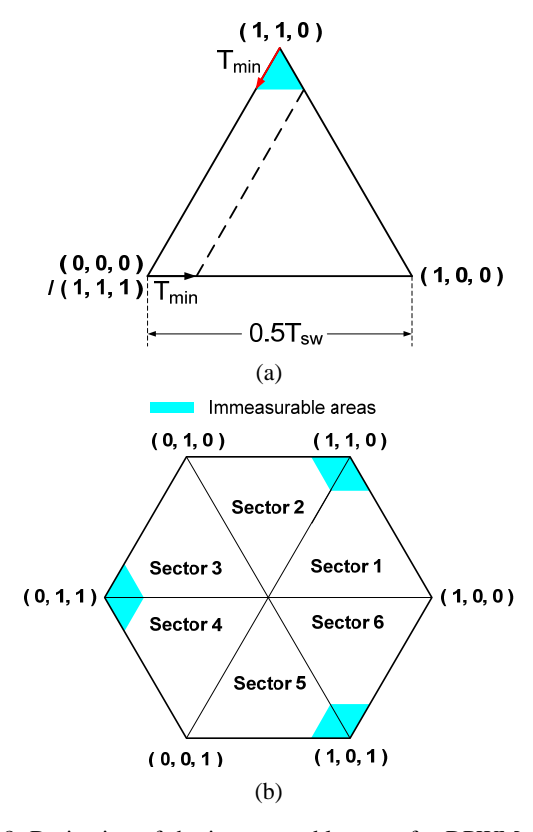


Fig. 8. Derivation of the immeasurable areas for DPWM. : (a) Immeasurable area in sector 1, and (b) all immeasurable areas.

By applying DPWM, the zero vector (0,0,0) can be inserted instead of another zero vector (1,1,1) as shown in Fig. 7, and the immeasurable areas can be reduced. Equations from (4) to (6) provide the boundary conditions. The resultant areas are demonstrated in skyblue in Fig. 8.

$$T_{b} = T_{1} + 2T_{0} < T_{\min}$$
 (4)

$$2T_0 + T_1 + T_2 = \frac{T_{sw}}{2} \tag{5}$$

The result of equating (4) and (5), is as follows. :

$$T_2 > \frac{T_{sw}}{2} - T_{min} \tag{6}$$

B. Identification of the Boundary Areas

TABLE II
SYSTEM SPECIFICATION

STSTEM SPECIFICATION	
DC link (V _{dc})	300[V]
Load resistance (Rs)	5.5[Ω]
Load inductance (Ls)	41[mH]
Poles	48
Shunt resistance (Rshunt)	40[mΩ]
Switching period (Tsw)	62.5[us]
Minimum duration (Tmin)	8[us]
Operating frequency (f)	~ 480[Hz]

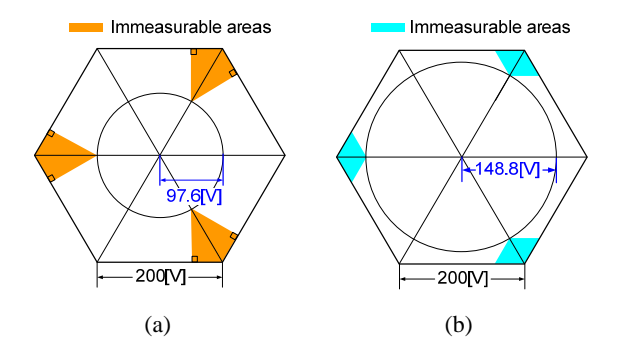


Fig. 10. Immeasurable areas for given system in the case of (a) SVPWM and (b) DPWM.

To verify the boundary derivation of TSSI, simulations were conducted with the system specifications (for a washing machine application) shown in Table II. Theoretically, the maximum magnitudes of voltage references with SVPWM and DPWM for accurate phase current reconstruction were determined to be 97.6[V] and 148.8[V[, respectively, as shown in Fig. 10.

The performance of the phase current reconstruction for each PWM method is presented in Fig. 11 and Fig. 12. For SVPWM, where there should be no error in the reconstructed phase currents when the magnitude of the voltage reference is less than 97.6[V], the reconstructed phase currents are assumed to be different from the actual phase currents when the magnitude of the voltage reference exceeds 97.6[V]. To confirm the failure of the reconstruction performance clearly, a comparatively high

voltage of 120[V] is applied. The reconstructed currents of the two phases show zero clamping phenomena, as shown in Fig. 11(b). This is the result when current sampling is conducted after the lower switch in the corresponding phase is turned off. If the resonance effect is included in the simulation, more realistic waveforms can be obtained. This is demonstrated in the experimental results.

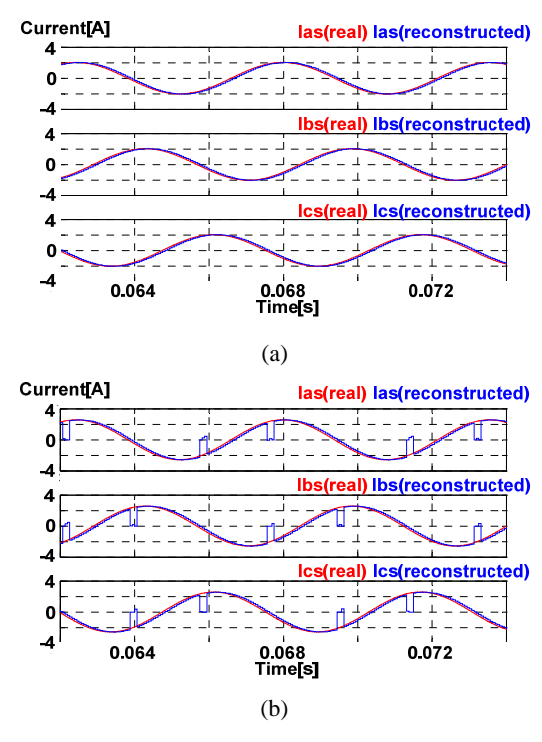


Fig. 11. Current reconstruction for SVPWM with different voltage reference magnitude of (a) r=95[V] and (b) r=120[V].

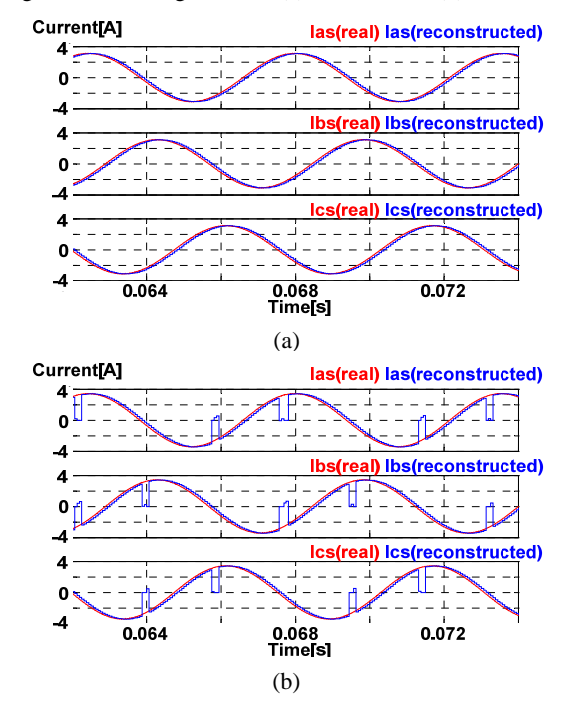


Fig. 12. Current reconstruction for DPWM with different voltage reference magnitude of (a) r=145[V] and (b) r=160[V].

III. EXPANSION OF MEASURABLE AREAS

The immeasurable areas derived previously can be reduced by a voltage injection and compensation. To minimize the ripple currents, the minimum voltage is injected and compensated. Basically, when the voltage reference is in an immeasurable area, it is relocated to a measurable area by means of a voltage injection.

A. Voltage Injection for SVPWM

To describe the voltage injection process, it is assumed that the reference voltage is in sector 1, for example. However, for other sectors, the same approach can be applied. As shown in Fig. 13, the immeasurable area can be divided into three sub-areas according to the different voltage injection modes. First, when the voltage vector lies in area S1, surrounded by $\Box ABFD$, voltage is injected as shown in Fig. 14(a), in which the line connecting the original point and the injected point is perpendicular to the measurable boundary line \overline{AD} . In this way, the magnitude of the injected voltage is minimized and, consequently, the current ripples resulting from the injection can be minimized.

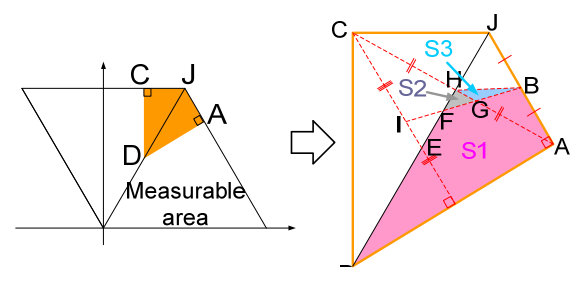


Fig. 13. Immeasurable area division for SVPWM.

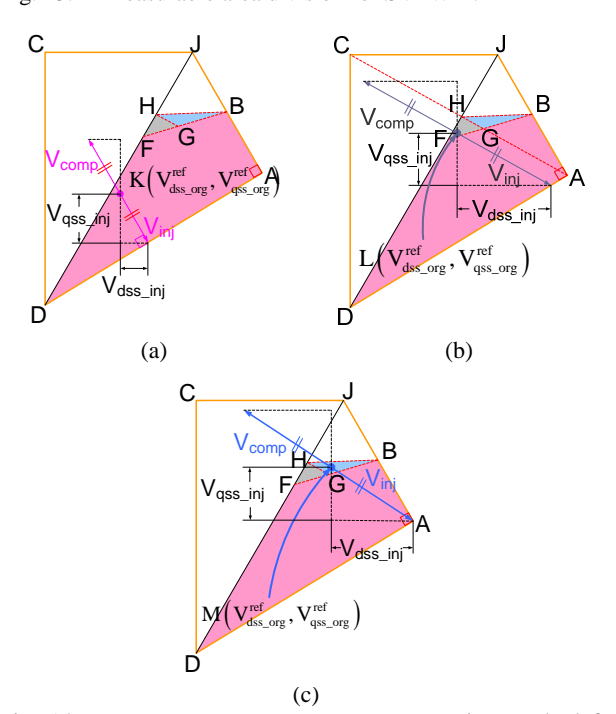


Fig. 14. Proposed voltage injection/compensation method for SVPWM when the original voltage reference is in (a) S1, (b) S2, and (c) S3.

If the same injection and compensation approach is applied when the voltage reference is in $S2(\triangle FGH)$ or $S3(\triangle BGH)$, the compensated voltage vector would be out of the hexagon and cannot therefore be synthesized by PWM. This leads to an imbalance between injection and compensation. Therefore, when the voltage vector lies in S2 or S3, another approach should be implemented.

When the reference exists in S2, voltage can be injected parallel to line \overline{AC} , as shown in Fig. 14(b); this is the minimum magnitude for perfect compensation. Similarly, when the reference is placed in S3, the nearest point for injection becomes the point A, as shown in Fig. 14(c).

B. Voltage Injection for DPWM

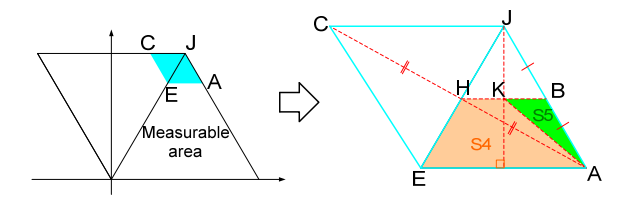


Fig. 15. Immeasurable area division for DPWM.

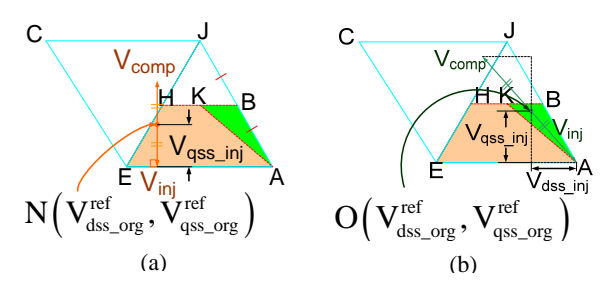


Fig. 16. Proposed voltage injection/compensation method for DPWM when original voltage reference is in (a) S4 and (b) S5.

Similar approaches can be adopted to expand the measurable areas for DPWM. The original immeasurable area is divided into two sub-areas, as shown in Fig. 15, depending on the voltage injection mode. When the original reference voltage vector is placed in S4(\square AEHK), the orthogonal point to line $\overline{\text{AE}}$ from the original reference point is optimal in terms of the minimum magnitude of the injection voltage. Therefore, when the original reference voltage vector is in sector 1, there is no injection voltage in the d-axis and only the q-axis injection voltage exists, as shown in Fig. 16(a). In the case of S5, point A is chosen for the injection to keep the compensated point within the voltage hexagon. This process is depicted in Fig. 16(b).

IV. SIMULATION AND EXPERIMENTAL RESULTS

The effectiveness of the proposed voltage injection method is verified in simulations and experiments. To evaluate the proposed method, the reconstructed phase current waveforms are compared to the actual phase currents. Fig. 20 shows the SVPWM simulation results,

where the magnitude of the voltage reference vector is 120 [V]. As shown in Fig. 20, the phase currents are accurately reconstructed compared to Fig. 11.

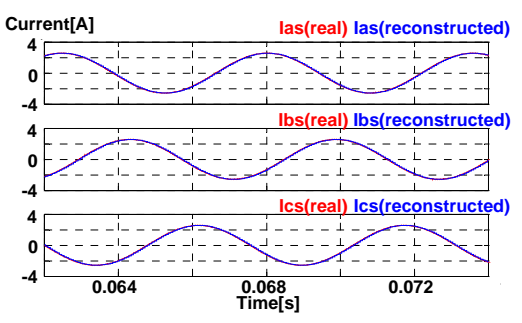


Fig. 20. Simulation results for the proposed method in SVPWM, where r=120[V] and f=180[Hz]. : Current waveforms reconstructed by the proposed method

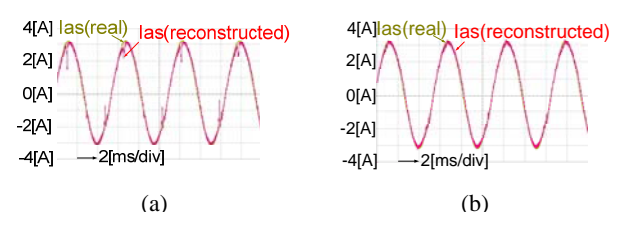


Fig. 21. Experimental results for the proposed method in SVPWM, where r=140[V] and f=180[Hz]. : (a) Current waveforms reconstructed without a voltage injection and (b) current waveforms reconstructed with a voltage injection.

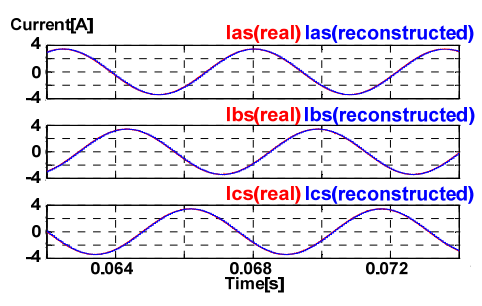


Fig. 22. Simulation results for the proposed method in DPWM, where r=160[V] and f=180[Hz]. : (a) Current waveforms reconstructed by the proposed method, (b) the injected voltages and (c) the final voltage reference locus.

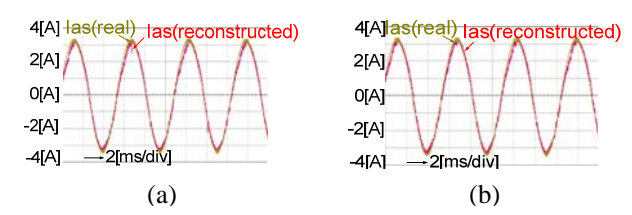


Fig. 23. Experimental results for the proposed method in SVPWM, where r=155[V] and f=180[Hz]. : (a) Current waveforms reconstructed without a voltage injection and (b) current waveforms reconstructed with a voltage injection.

The experimental results in Fig. 21 support the validity of the proposed method for SVPWM. When the voltage reference with a magnitude of 140 [V] is applied without a voltage injection, the current of phase 'a' is erroneously

reconstructed, as shown in Fig. 21(a). However, the reconstruction performance greatly improves, as shown in Fig. 21(b).

For DPWM, the proposed method was also confirmed, as shown in Fig. 22 and Fig. 23. The phase current reconstruction performance is satisfactory in both the simulation and the experimental results.

V. CONCLUSION

In this paper, the boundary conditions for phase current reconstruction of a three-shunt sensing inverter (TSSI) were analytically derived. This paper proposes a voltage injection method for the enhancement of phase current reconstruction in immeasurable areas, providing that the immeasurable areas are reduced in SVPWM and DPWM. To minimize the side effects of a voltage injection, the minimum magnitude voltage is selected. The effectiveness of the proposed method is verified by simulations and experimental results.

REFERENCES

- [1] Chucheng Xiao, Lingyin Zhao, Asada T., Odendaal W.G. and van Wyk J.D., "An overview of integratable current sensor technologies," Industry Applications Conference, 2003, vol. 2, pp. 1251-1258
- [2] S.Chakrabarti, T.M.Jahns and R.D.Lorenz, "A Current Reconstruction Algorithm for Three-Phase Inverters Using Integrated Current Sensors in the Low-Side Switches," Industry Applications Conference, 2003, vol. 2, pp. 925-932
- [3] S.Chakrabarti, T.M.Jahns and R.D.Lorenz, "Reduction of Parameter Sensitivity in an Induction Motor Current Regulator Using Integrated Pilot Sensors in the Low-Side Switches," Industry Applications, IEEE Transactions on, vol. 41, pp. 1656-1666, 2005
- [4] S.Chakrabarti, T.M.Jahns and R.D.Lorenz, "A Current Control Technique for Induction Machine Drives Using Integrated Pilot Current Sensors in the Low-Side Switches," Power Electronics, IEEE Transactions on, vol. 22, pp. 272-281, 2007
- [5] T.C.Green and B.W.Williams, "Derivation of motor line-current waveforms from the DC-link current of an inverter," Electric Power Applications, IEE Proceedings B, vol. 136, pp. 196-204, 1989
- [6] Jung-Ik Ha, "Voltage injection method for threephse current reconstruction in PWM inverters using a single sensor," *IEEE Trans. Power Electron.*, vol. 24, no. 3, pp. 767–775, Mar. 2009
- [7] Byung-Geuk Cho, Jung-Ik Ha and Seung-Ki Sul, "Voltage Injection Method for Boundary Expansion of Output Voltages in Three shunt Sensing PWM Inverters," Power Electronics and ECCE Asia (ICPE & ECCE), 2011 IEEE 8th International Conference on, pp. 411-415